Hyperthermia of Magnetic Nanoparticles: An Experimental Study of the Role of Aggregation

Clément Guibert, Vincent Dupuis, Véronique Peyre, Jérôme Fresnais

Hyperthermia of magnetic nanoparticles: an experimental study of the role of aggregation

*Clément Guibert, Vincent Dupuis, Véronique Peyre, and Jérôme Fresnais**

[1]Université Pierre et Marie Curie-Paris 6, UMR 8234, PHENIX, CNRS, Paris, F-75005 France;

*Corresponding author. Université Pierre et Marie Curie-Paris 6, UMR 8234, PHENIX, CNRS, Paris, F-75005 France; Email: jerome.fresnais@upmc.fr

ABSTRACT:

Magnetic hyperthermia is a promising tool as an adjuvant therapy for multimodal cancer treatment. However, the heating efficiency of magnetic nanoparticles in biological conditions is not yet fully understood, especially regarding their dispersion state. In this work, dynamic light scattering (DLS) and hyperthermia experiments were coupled to highlight the role of the aggregation of iron oxide nanoparticles on their heating properties induced by an alternating magnetic field. Bare, poly(acrylic acid), and poly(acrylic acid-co-maleic acid) coated nanoparticles were studied. More precisely, the interparticular interactions were investigated by varying the ionic strength and the pH. Our results show that the specific loss power (SLP) of nanoparticles in small and loose aggregates is similar to that of well dispersed nanoparticles while the formation of large and dense aggregates observed by DLS can be correlated to a decrease of the SLP of the nanoparticles. However, at intermediate aggregation states, DLS experiments alone do not allow to fully comprehend the heating properties of magnetic nanoparticles. Small angle X-ray scattering experiments (SAXS) were performed to get information about the inner structure of the aggregates: the closer the nanoparticles in the aggregates, the less they heat the surrounding medium. These results shed a new light on the negative influence of the interparticular interactions in aggregates on the particles heating efficiency.

KEYWORDS:

Iron oxide nanoparticles, maghemite, hyperthermia, dynamic light scattering, Small Angle X-Ray Scattering, aggregation, interparticular interactions

INTRODUCTION

Magnetic hyperthermia is a phenomenon of great interest for materials and medicine applications. Indeed, the ability to convert electromagnetic energy into heat at a nanoscale with magnetic nanoparticles (NPs) opens up new perspectives for various applications. The best known is probably the destruction of tumor cells by heating them up to their apoptosis threshold. This strategy is currently under development [1–4] and it uses simple theoretical models that have been developed during the past decade [5]. Alternative strategies in cancer treatment using heating induced by an alternating magnetic field are also emerging. They propose to use heating at the nanoscale to release drug molecules in their surrounding environment [6,7].

If Rosensweig's model [5] is very efficient to predict basic features of hyperthermia, it does not yet take into account the complexity of the surrounding medium in which the NPs are immersed. For instance, on the one hand, Haase & Nowack [8] demonstrated that magnetic dipolar interactions between NPs in a ferrofluid of increasing NPs concentration have a negative influence on the heating power (also often called specific loss power (SLP)). On the other hand, Mehdaoui *et al.* [9] showed through simulations that the same dipolar interactions between NPs of low magnetic anisotropy could lead to an increase of the SLP. These studies on model systems show the importance of the mean interparticular distance between the NPs on their heating efficiency, but the mechanisms of this influence are little described and understood. Despite this lack of knowledge on complex systems where nanoparticles interact, this question rarely is the main subject of studies. This fact is underlined in a recent review [10] and experimental studies refer to these misunderstood interactions to explain noteworthy unexpected results for complex systems. For instance, it has been reported that NPs highly concentrated in liposomes see their SLP increase [11], whereas other authors report a decrease of the SLP of NPs confined in a polystyrene matrix [12]. Moreover, de *Sousa et al*. suggested that the dispersion state of NPs could affect their SLP by showing that NPs functionalized with citrate ligands have a reduced heating efficiency [13].

In this study, we intend to highlight the relationship between the dispersion state of NPs and their heating power in water through different model systems consisting of maghemite nanoparticles with an average diameter of approximately 12 nm and with three different surface functionalizations : native surface (positively charged) and surface functionalized either with poly(acrylic acid) or with poly(acrylic acid-co-maleic acid). The first system will be used as a reference system to put forward the role of the functionalization. The latter systems are particularly interesting for their tunable aggregation controlled by the pH and their broad domain of colloidal stability in terms of ionic strength [14].

MATERIALS AND METHODS

Materials

Magnetic nanoparticles (NPs)

Aqueous dispersions of maghemite NPs (γ-Fe_2O_3) were synthesized by coprecipitation following Massart's synthesis pathway [15]. The NPs size polydispersity was then reduced by size sorting based on destabilization of the dispersion by an increase of the ionic strength [16]. The final pH is around 1.8, ensured by nitric acid.

The size and polydispersity of the NPs were characterized by TEM (fig. 1). The analysis of the pictures lead to a normal size distribution of median diameter d_0 = 11.7 nm and a standard deviation value of 3.7 nm. These values are in good agreement with DLS and magnetization measurements (SI-1).

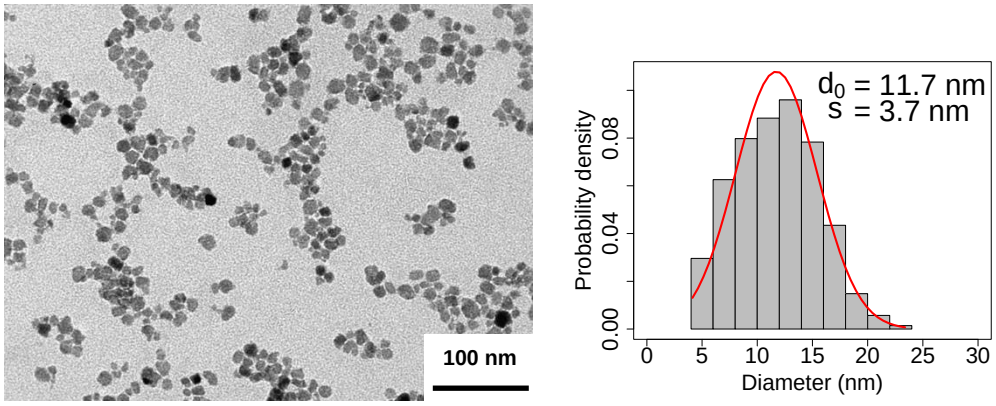

Figure 1: Left: TEM picture of the NPs; right: size distribution obtained by TEM pictures analysis (red line: normal distribution model, with d_0 = 11.7 nm and standard deviation of 3.7 nm)

The concentration of the maghemite nanoparticles in the dispersions was measured with two techniques. Measurements of the iron content (after dissolution of the NP by concentrated HCl) were performed by atomic absorption spectroscopy (Aanalyst 100, Perkin-Elmer). Maghemite content was also obtained by UV-visible spectroscopy with the help of a master-curve (between 450 and 700 nm [17]) for dispersions diluted in water (Avaspec 2048/Avalight DHC, Avantes). Both methods lead to coherent results.

Nanoparticles coating

Two types of functionalization were studied: polyacrylic acid (PAA) and poly(acrylic acid-co-maleic acid) (PAAMA) (1:1 mole ratio of (acrylic acid):(maleic acid)) coatings. PAA (sodium salt, 2100 g.mol^{-}

[1], Sigma-Aldrich), and PAAMA solution (3000 g.mol^{-1}, 50 wt. % in H_2O, Sigma-Aldrich) were used as received. Both coatings were performed by precipitation-redispersion following the procedure described for PAA in [18].

Acidity & ionic strength control

An automatic titrator (MTP2 autotitrator, Malvern) was used to adjust the pH or the ionic strength of the samples. The acidity of the solutions was adjusted by adding 0.10 mol.L^{-1} nitric acid or tetramethylammonium hydroxide solutions (TMAOH). The ionic strength of the solutions was adjusted by adding concentrated (1.0 to 5.0 mol.L^{-1}) ammonium chloride solutions. These solutions were prepared by dissolution of ammonium chloride (NH_4Cl, Sigma-Aldrich, used as received) in distilled water.

Dynamic Light Scattering (DLS) & Specific loss power (SLP) measurements

A DLS apparatus (Malvern Nano-ZS, wavelength λ = 656 nm, scattering angle θ = 173°) and a commercial generator of oscillating magnetic field (magneTherm, nanoTherics, alternating magnetic field at 333 kHz with an amplitude of 9 mT) were set up in series. The circulation of the sample through the two measuring cells was ensured by the peristaltic pump of the MPT2 autotitrator in order to record concomitantly the hydrodynamic diameter of the objects dispersed in water and their SLP (fig. 2). DLS intensity autocorrelation functions ($G_2(t)$) were fitted by the sum of two exponential functions to extract the contributions of isolated and aggregated nanoparticles (eq 1). Note that the contributions are thus considered as intensity weighted ones.

$$G_2(t) = A_0 + A_1 e^{-2D_1 q^2 t} + A_2 e^{-2D_2 q^2 t} \qquad (1)$$

where A_0 is a constant corresponding to uncorrelated fluctuations, A_1 and A_2 are the intensity weights of isolated and aggregated NPs, respectively. Coefficient D_1 and D_2 correspond to the diffusion coefficients of isolated and aggregated NPs, respectively. They are related to the hydrodynamic diameter d_H using the Stokes-Einstein equation: $d_H = \frac{kT}{3\pi\eta D_i}$. q is the scattering vector, defined as $q = \frac{4\pi n}{\lambda}\sin(\theta/2)$, with n the refractive index of the solvent, λ the laser wavelength, and θ the scattering angle.

The isolated nanoparticles diameter was set as the first contribution to the fit. A_0, A_1, A_2, and d_{H2} were adjusted to fit the experimental data $G_2(t)$ with equation 1. The intensity-weighted contributions of isolated ($\%_{isolated}$) and aggregated ($\%_{aggregated}$) NPs were determined using equation 2.

$$\%_{islotaed} = \frac{A_1}{A_1 + A_2}; \%_{aggregated} = \frac{A_2}{A_2 + A_1} \quad (2)$$

The average diameter was then calculated with the intensity-weighted contribution of each diameter (eq 3, SI-2).

$$d_{H\,ave} = \%_{isolated}{}' \; d_{H\,isolated} + \%_{aggregated}{}' \; d_{H\,aggregated} \quad (3)$$

After adding a solution in the main reservoir, the dispersion was pumped through the whole loop for about 5 minutes to homogenize the dispersion, which allows to recirculate approximately 10 times the total sample volume. The pump then stopped and the temperature was monitored in the SLP measurement cell. A temperature equilibrium lasting at least 30 seconds was required prior to performing DLS and SLP measurements. The volume of solution added to the sample was controlled by the autotitrator and accurately recorded. The dilution induced by the addition of solution was taken into account to calculate the exact NPs concentration during the whole experiment.

A non-metallic optical fiber thermometer (Fluoroptic, Luxtron) was used to record the temperature evolution in the samples induced by the application of an oscillating magnetic field. The initial rise of temperature was approximated by a linear increase as a function of time (dT/dt). The SLP of the nanoparticles in the sample was then calculated according to equation 4:

$$SLP = C_P \times w \times \frac{dT}{dt} \quad (4)$$

where C_p is the specific heat capacity of the solvent and w is the weight fraction of NPs in the sample. A value of $C_p = 4184$ $W.K^{-1}.g^{-1}$ was used in water.

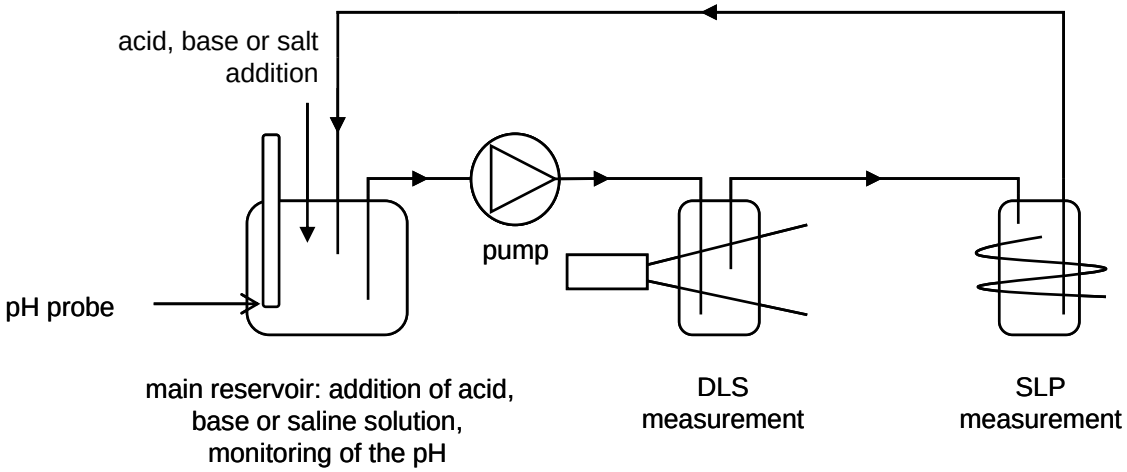

Figure 2: Schematic of the coupling of DLS and SLP measurements

SAXS experiments

Different dispersions were analyzed by small angle X-ray scattering (SAXS) measurements on the SWING beamline of the SOLEIL Synchrotron (Saint Aubin, France). The measurements were performed at an energy of 7 keV (λ = 1.77 Å), with a two dimensional CCD detector localized at a distance of 3.5 or 1 m from the sample in order to achieve a scattering vector (Q) range of 0.002 $Å^{-1}$ – 0.3 $Å^{-1}$. Standard correction procedures were applied for sample thickness, X-ray beam transmission, empty cell signal subtraction, and detector efficiency to obtain the scattered intensity in absolute scale (cm^{-1}). The software *Foxtrot*® was used to achieve such data reduction.

The samples for SAXS were prepared by batch, by adding some base (resp. acid) to initial dispersions of bare NPs (resp. coated NPs) until the desired pH was reached.

RESULTS

1) Effect of ionic strength:

Bare NPs are easily destabilized by an increase of the ionic strength. Typically, for a dispersion containing 4 wt. % of NPs, above a concentration of 0.4 mol L^{-1} of nitric acid, more than 50 % of the NPs are flocculated [16]. Therefore, only PAA and PAAMA coated NPs have been studied in this paragraph. Their SLP and hydrodynamic diameter are plotted versus NH_4Cl concentration on fig. 3. This figure shows that PAA coated NPs are stable on the whole range of investigated ammonium chloride concentrations since the hydrodynamic diameter remains constant (around 45 nm), from 0.001 to 1.0 mol L^{-1}. This is consistent with previous results [14]. Concomitantly, the SLP also remains constant in the whole ionic strength range.

Regarding PAAMA coated NPs, a strong aggregation (characterized by a steep increase of the hydrodynamic diameter) is triggered when the ionic strength reaches a value between 0.10 $mol.L^{-1}$ and 0.50 $mol.L^{-1}$. Simultaneously, a decrease of 45 % of the SLP is observed.

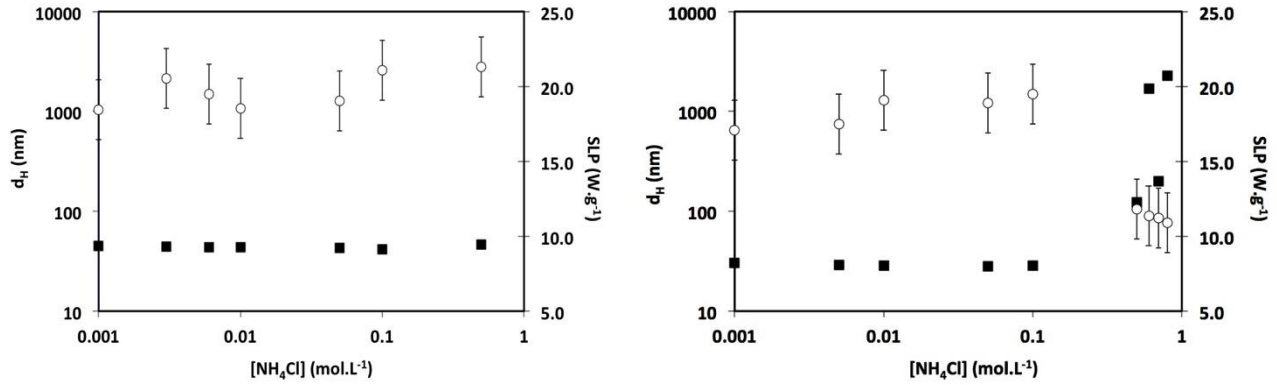

Figure 3: SLP (open circles – right scale) and hydrodynamic diameter, d_H, (filled squares – left scale) versus NH_4Cl concentration. Left: PAA coated NPs, right: PAAMA coated NPs, (maghemite mass fraction: 0.5 to 0.3 wt. %).

2) Effect of pH :

The aggregation of the NPs was controlled by varying the pH. Indeed, this parameter changes the charge density of the native surface or of the polymer coating through acid-base reactions. It is thus possible to tune the charge born by the NPs, that is responsible for the interparticular repulsions. The total ions concentration in the samples remained below 0.05 mol.L^{-1}. Under these conditions, the aggregation is mainly due to pH variations rather than ionic strength variations, even for bare nanoparticles.

a. Bare NPs

The results obtained for bare nanoparticles are reported on figure 4. Starting from acidic pH, the dispersion was progressively destabilized by adding a base, TMAOH. DLS was used to record correlation functions $G_2(t)$ at the different pH. From $G_2(t)$, we determined for each pH both the average hydrodynamic diameter and the contribution and hydrodynamic diameter of isolated well dispersed (22.2 nm) and aggregated nanoparticles. The size of the aggregates was estimated at 56 nm between pH 2.1 to 3.8. It increased then progressively from 80 nm at pH = 4.5 up to 230 nm at pH = 5.3. A complete aggregation is observed at pH 7.1, with no isolated detectable nanoparticle and large aggregates that tend to flocculate. Note that at pH 7.1, the micrometric size determined with DLS is unsignificant.

Between pH 2.1 and 3.8, the analysis of the correlation functions highlight the growing contribution of the aggregates (from 7% to 47%) to the scattered intensity, and the diminution of the contribution of isolated nanoparticles (from 93% to 53%). For pH values above 3.8, aggregates become larger and their contribution is preponderant in the solution.

Interestingly, the SLP of the nanoparticles remains constant from pH 2.1 to 5.5 (around 20 $W.g^{-1}$). An SLP decrease is detected at pH 7.1, where a complete aggregation of the NPs is observed, with no isolated NPs detected.

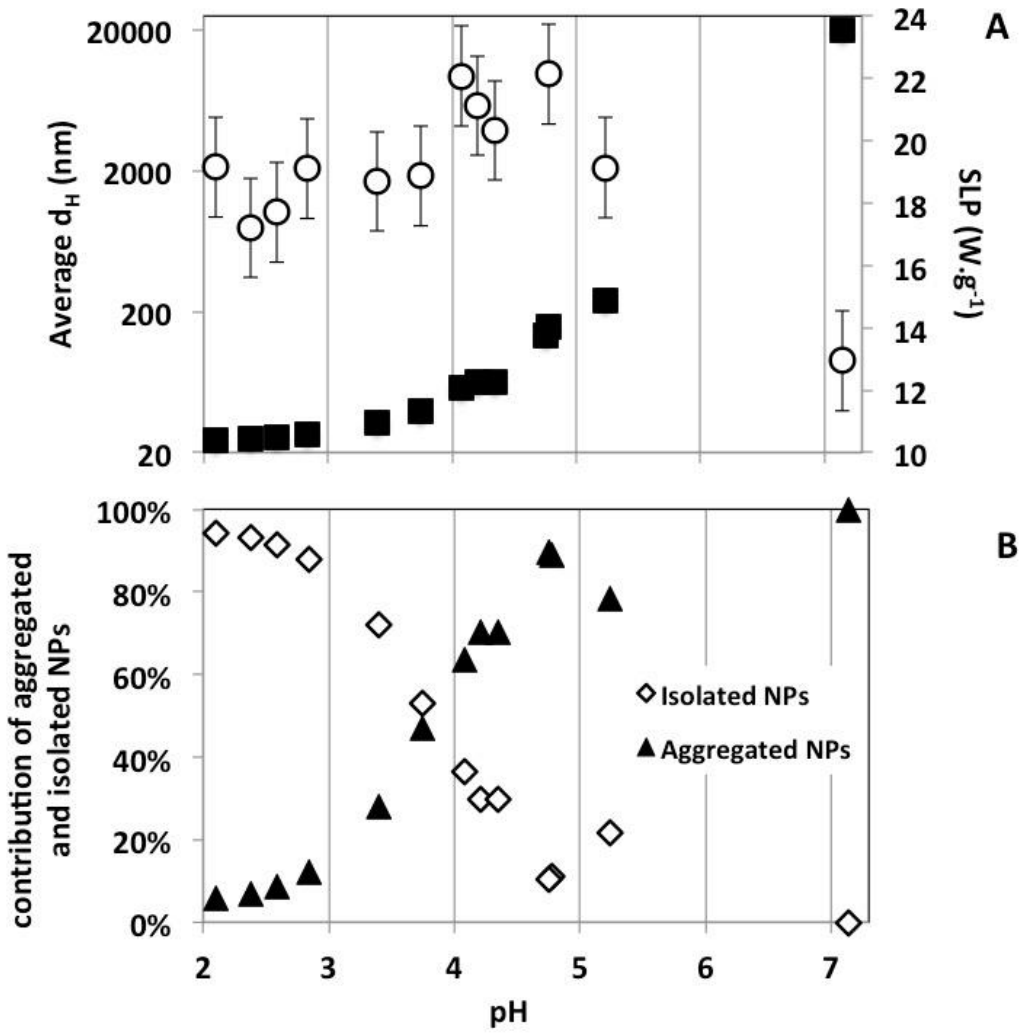

Figure 4: A: SLP (open circles-right scale) and average hydrodynamic diameter, d_H, (filled squares- left scale) versus pH for bare nanoparticles (maghemite mass fraction: 0.40 to 0.37 wt. %) – B: Relative contributions of isolated NPs ($\%_{isolated}$, open diamonds) and aggregates ($\%_{aggregated}$, triangles) versus pH

b. PAAMA coated NPs

The same experiment was achieved for PAAMA coated NPs, starting from pH 7 down to 1.5. According to the average diameter, PAAMA coated NPs are stable over a large pH range, from pH 7 to 2.8 (figure 5). However, between 3.2 and 2.8, small aggregates (smaller than 60 nm) are detected (fig. 5 down). They do not influence the SLP, that remains constant (20 $W.g^{-1}$) down to pH = 2.8. Then, an abrupt decrease of the SLP is measured, from 20 $W.g^{-1}$ to 6 $W.g^{-1}$ between pH = 2.8 and 1.5, while the sizes and the contribution of the aggregates increase drastically.

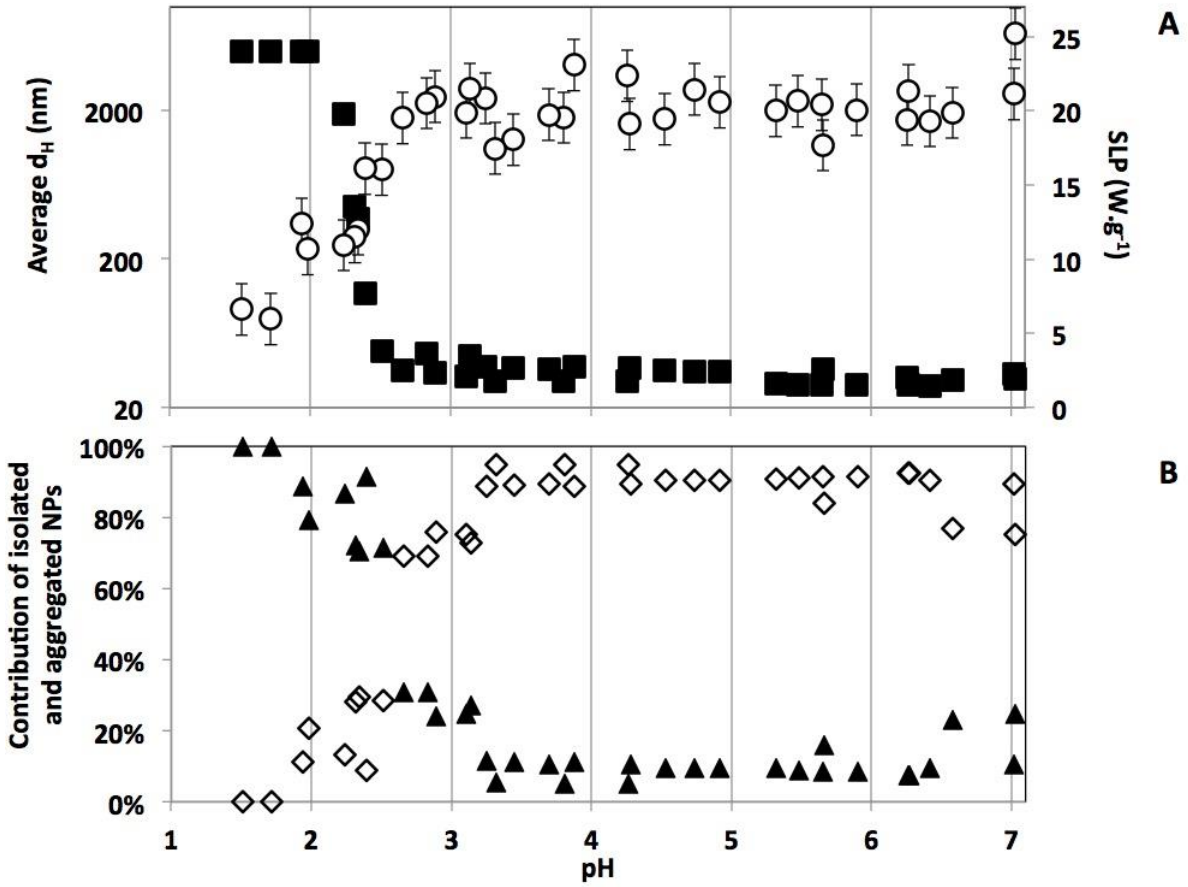

Figure 5 A: SLP (open circles – right scale) and averaged hydrodynamic diameter, d_H, (filled squares – left scale) versus pH for PAAMA coated nanoparticles (maghemite mass fraction: 0.45 to 0.30 wt%) – B: Relative contributions of isolated NPs ($\%_{isolated}$, open diamonds) and aggregates ($\%_{aggregated}$, triangles) versus pH

c. PAA coated NPs

A similar experiment was achieved with PAA coated NPs, starting from pH 8.1 (fig.6).

Contrary to bare and PAAMA NPs, aggregates around 70 nm are initially present ($\%_{aggregated}$ around 30 %), which corresponds to very small aggregates of 2-3 NPs, probably formed during the coating process. They remain stable afterwards. Interestingly, the initial slight aggregation does not influence significantly the SLP values, which is equal to that of well dispersed bare or PAAMA coated NPs.

The titration of PAA coated NPs induces no further aggregation while decreasing pH from 8.1 to 4.5 (fig. 6), as evidenced by the constant contribution of aggregates and the constant d_H. Between pH 4.5 and 3.8, a slight aggregation occurs ($\%_{aggregated}$ and d_H increase). This has no influence on the SLP. Then, the average hydrodynamic diameter increases sharply from pH 3.8 to 2.5, where a flocculation is observed.

A decrease of the SLP is only detected when aggregates are large and preponderant in the dispersion, at pH lower than 3.5. Contrary to PAAMA coated NPs where the minimum SLP value was 5 $W.g^{-1}$, the SLP of PAA coated NPs decreases only from 20 to 10 $W.g^{-1}$.

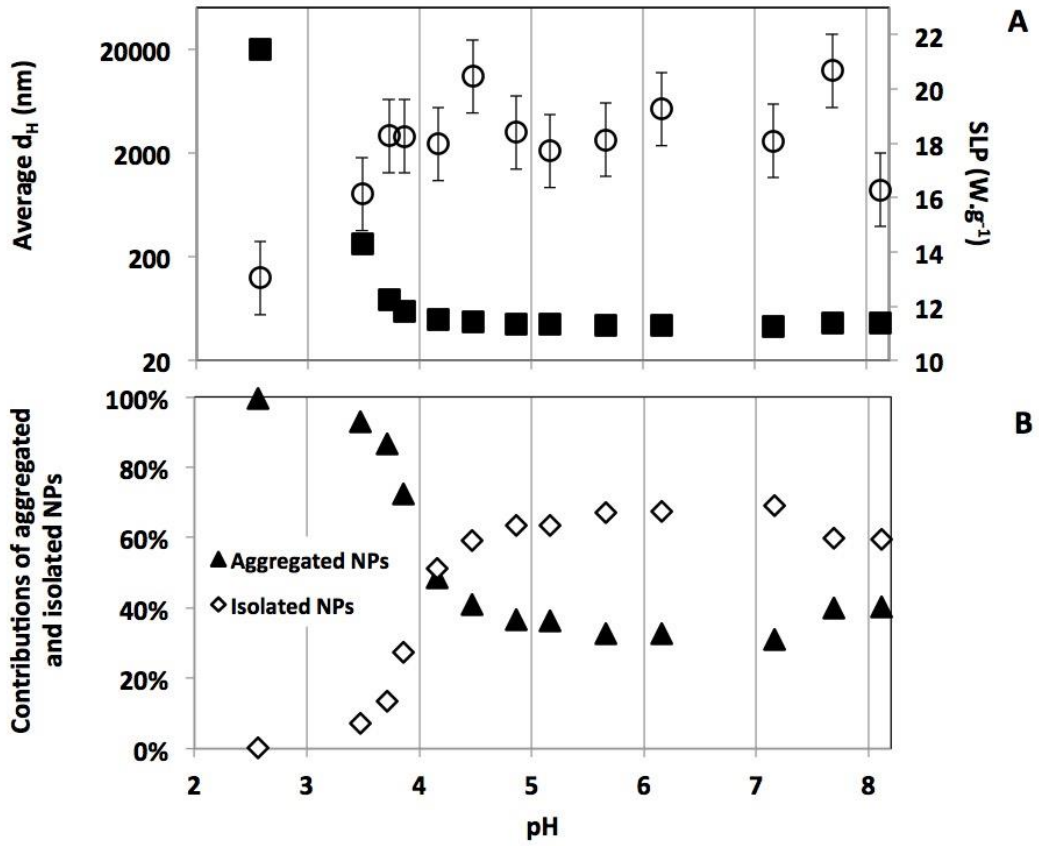

Figure 6: A: SLP (open circles – right scale) and hydrodynamic diameter, d_H, (filled squares-left scale) versus pH for PAA coated nanoparticles (maghemite mass fraction: 0.45 to 0.30 wt. %) – B: Relative contributions of isolated NPs ($\%_{isolated}$, open diamonds) and aggregates ($\%_{aggregated}$, triangles) versus pH

DISCUSSION

Colloidal stability and SLP

a) Colloidal stability

We first investigated the stability of PAA and PAAMA coated NPs as a function of the ionic strength. PAA coated nanoparticles are stable up to 1.0 mol.L^{-1} of NH_4Cl, while PAAMA coated NPs are stable at ionic strengths below 0,1 mol.L^{-1}. This stability can be explained by the number of charges per unit of NPs surface, that increases drastically (roughly 20 titrable groups per square nanometer for PAA [17,18]) in comparison to bare NPs (1.5 charge.nm^{-2}). This strengthens the electrostatic repulsions that persist even at high ionic strength[19,]. This is an important result, as *in vivo* conditions often involve high ionic strengths and it is difficult to stabilize such NPs because of their small surface over volume ratio. Surprisingly, we found that PAAMA coated NPs were more sensitive to the ionic strength, which had never been demonstrated before. The difference between PAA and PAAMA is probably due to their different structures and conformation at the NPs surface.

As a reference, we chose to study the aggregation of bare NPs with native surface charges when the pH is increased and its influence on the SLP. At acidic pH (*i.e.* below the point zero charge of 7), these NPs bear surface oxonium groups, $–OH_2^+$, which ensures the colloidal stability of the dispersion through electrostatic repulsive interactions. DLS measurements indicate that the aggregation remains limited from pH 2 up to 4. When the pH is increased, these groups are deprotonated and the surface becomes neutral. The remaining interparticular interactions are then purely attractive (van der Waals and magnetic interactions) and the NPs flocculate. Interestingly, the SLP remains constant until the complete aggregation of the bare NPs is observed. Thus, the precise role of the aggregation cannot be clearly elucidated by using DLS experiments only since the partial aggregation of the NPs measured by DLS does not induce a significant effect on the hyperthermia efficiency in this case.

The two kinds of coated NPs display a similar behavior in terms of colloidal stability. Indeed, they both bear the same functional groups: carboxylic acids. At basic pH, these groups are deprotonated and display a negative charge ($-COO^-$). Only their molecular weight and their linear charge density vary between PAA and PAAMA. These groups ensure the colloidal stability of the dispersion through electrostatic repulsive interactions. If PAAMA coated NPs are well dispersed at basic pH, PAA coated

NPs exhibit a contribution to the scattered intensity that can be attributed to the presence of small aggregates made of 2-3 NPs. Their formation does not influence the SLP values, which is identical to that of uncoated or PAAMA coated NPs when well dispersed (almost 20 $W.g^{-1}$).

As for the pH effect on the PAA or PAAMA coated NPs, a sudden aggregation of the coated NPs was observed when decreasing the pH (below 4.0 for PAA, below 2.6 for PAAMA). This occurs over a very narrow pH range (1 pH unit), contrary to bare NPs that aggregate over more than 3 pH units.

A similar effect of aggregation is noticed for uncoated and PAA coated NPs on their SLP. Namely, the SLP value decreases from 20 $W.g^{-1}$ to 10 $W.g^{-1}$, from well dispersed to fully aggregated states. For PAAMA coated nanoparticles, the decrease is even more significant: a decrease from 20 W g^{-1} to 5 W g^{-1} is measured between the two extreme pH values.

SAXS experiments:

In order to get a better insight into the structure of the aggregates, SAXS experiments were performed to characterize more precisely the NPs aggregates and to get a finer description of the interparticular interactions.

The reference diffractogram for non-aggregated and non-interacting bare NPs at pH = 1.9 can be fitted by the form factor of a normal distribution of polydisperse hard spheres (mean diameter: 10.8 nm, standard deviation 4.1 nm, SI-3), in good agreement with TEM analysis. Experimental structure factors were calculated by dividing the diffractograms by this experimental form factor of well dispersed nanoparticles.

For the three systems, we focused on the two extreme states, *i.e.* well dispersed NPs displaying the highest SLP and aggregated NPs displaying the lowest SLP (figure 7).

For bare and PAAMA coated NPs, the well dispersed state is characterized by the same form factor. In the case of PAA coated NPs, an increase of the scattered intensity at small Q is observed. The corresponding aggregation number can be calculated by dividing the asymptotic value of the scattered intensity for Q = 0 by the similar value obtained for the form factor. A number of 3 is obtained, which is coherent with DLS measurements.

The SAXS diffractograms of aggregated states indicate for the different systems (bare, PAA, and PAAMA coated NPs) an aggregation (increase of the intensity at very low Q) into objects that are bigger than 300 nm, that is the maximal characteristic size possibly measurable, which corresponds to the

smallest accessible Q. For bare NPs, the exponent n = 2.1 of the initial power law $I \alpha Q^n$ can be taken as an indication of the low compactness of fractal aggregates. This is confirmed by the very small and smooth interaction peak displayed by the structure factor, around $Q^* = 0.052$ Å^{-1}, that is the reciprocal length of $d^* = 2\pi/Q^* = 12.1$ nm. d* can be interpreted as the mean contact distance between two NPs, that amounts to the diameter of a single particle (11.7 nm). The aggregation is achieved without conspicuous local structuring: the mean interparticular distance does not appear to be well defined for these loose fractal aggregates.

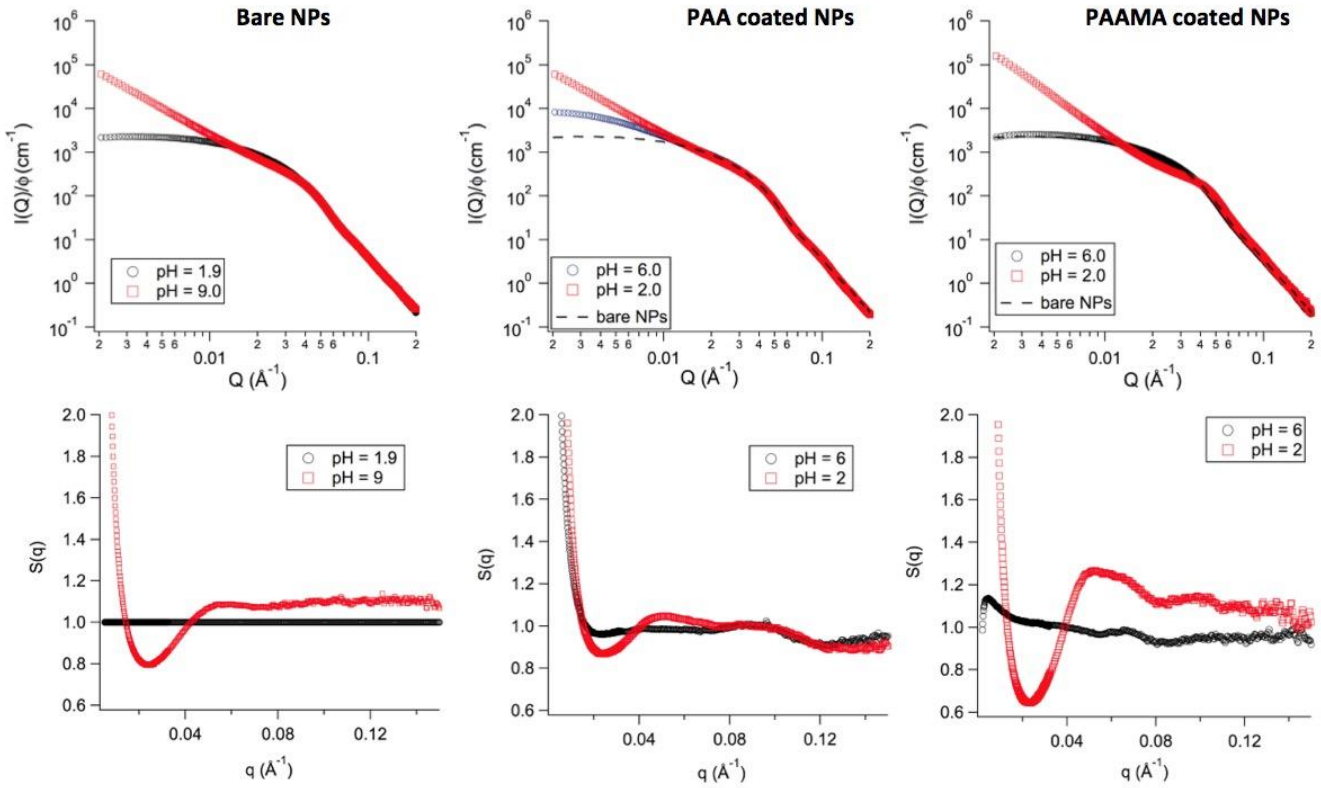

Figure 7 : SAXS diffractograms (up) and structure factors (down) of bare (left), PAA (middle), and PAAMA (right) coated NPs at two pH values (well dispersed (black circles) and aggregated (red squares) states). Maghemite mass fraction around 0.5 wt. %.

For PAA coated NPs (slightly aggregated at pH = 6; figure 7, middle), lowering the pH induces further aggregation, as seen on the diffractogram at pH 2. Similarly to bare NPs, the initial exponent of the power law is around 2.1. The small and smooth interaction peak in S(q) leads to a mean contact distance of about 12.6 nm, slightly higher than for bare NPs due to the adsorbed polymer layer.

For PAAMA NPs, upon the decrease of pH, the formation of denser aggregates can be noticed with an increase of the scattered intensity at low Q, with an initial power exponent of 2.4 at pH 2. In the intermediate Q range (0.02 A^{-1} < Q), the scattering of the large structures, which is preponderant at small Q, is dominated by the scattering of objects organized at a smaller scale. In this Q range, the experimental structure factor can be modeled as an dispersion of hard spheres of 0.10 - 0.15 volume fraction. This leads to the appearance of a sharp interaction peak at q* = 0.052 $Å^{-1}$, corresponding to d* = 12.1 nm. This d* value is again close to the contact distance between two NPs, with a denser packing than for PAA coated NPs.

b) SLP

Several conclusions can be drawn from this work concerning the influence of the aggregation on the SLP.

Firstly, in the systems studied here, the maximum SLP does not depend on the coating on the NPs. Indeed, the same values were measured for bare, PAA coated and PAAMA coated NPs when well dispersed. As long as no aggregation was observed, the ionic strength did not influence the SLP either. This screening of the long-range electrostatic interactions does not have an effect on heating efficiency, which had not been not clearly evidenced yet. It can be easily understood since the electrostatic repulsions are not explicitly related to the hyperthermia mechanisms.

Secondly, we demonstrated here an important correlation between the aggregation state and the SLP of the NPs. The aggregation of NPs induces an increase of magnetic interactions between nanoparticles, resulting in certain conditions in a decrease of hyperthermia efficiency. These interactions can be twofold. Magnetic dipole-dipole interactions such as modeled in [8] and [20]ref 22 plutôt ! (tan et al) can lead to a decrease of the heating efficiency of NPs. Here, the local concentration of NPs in the aggregates deduced from the SAXS (volume fraction around 0.10-0.15) corresponds to a concentration at which a significant decrease of the SLP can be expected, according to the simulations performed by Tan & al. [21]. Another factor should be taken into account: the demagnetization field. It is indeed induced inside the aggregates by their own magnetization and it reduces the local magnetic field, which leads, therefore, to a decrease of the SLP.

The results presented in this article can be summarized by the next three points. Firstly, when only small oligomers made of a few particles are formed (an aggregation number of 3 was found for PAA coated NPs), the SLP does not differ from a well-dispersed state. In this case the NPs are not numerous enough in the aggregates to cause strong enough interactions to affect the SLP.
Secondly, in some cases, the hydrodynamic diameter measured by DLS increases whereas the SLP remains constant. This effect is particularly noticeable in the case of bare NPs where the aggregation processes over 3 pH units but can also be observed for PAA and PAAMA NPs. It could be explained either by the small number of particles in aggregates or by a loose structure at the early stages of aggregation in which the NPs are too far from each other to interact strongly, as magnetic dipolar interaction energy decreases as a function of the distance between the particles centers to the power of 3 [22]. In the limit case of strong magnetic coupling, for 10 nm particles, this interaction can be estimated at - 1.2 kT when NPs touch and - 0.15 kT when at a distance of 20 nm. Thus, this becomes rapidly negligible compared to the thermal energy.

Thirdly, the SLP decreases drastically when the aggregates grow denser. This occurs when the neutralization of the NPs surface is complete or when the repulsive electrostatic interactions are completely screened for PAAMA coated NPs. The negative influence of the magnetic dipolar interactions between NPs in the aggregates then reach their maximum because the nanoparticles are in contact. It results in a significant decrease in SLP, all the more important that the inner structure of the aggregates is compact.

CONCLUSION

In this study, the coupling between DLS and SLP measurements led to the discovery of a correlation between the aggregation state and the heating properties of the NPs. Indeed, we showed that, whatever the nature of the surface of the NPs (coated or not), their colloidal stability and the morphology of the aggregates must be taken into account to comprehend the evolution of their SLP. Nonetheless, the indication we obtained by DLS about the aggregation is not sufficient to explain the SLP measured simultaneously. Comparing DLS and SAXS experiments highlights the different structures of the aggregates formed by varying the pH. While DLS data provide a good comprehension of the overall aggregation state, the precise inner structure of the clusters can be determined by using SAXS experiments.

Complementary studies are however necessary to link the strength of the aggregation, characterized by the compactness of the aggregates determined by SAXS, with the SLP decrease. These results can be of great interest for instance for biological application. The use of the PAA coating described here would enhance advantageously the stability of the NPs when used at a pH higher than 4.0. We hope that this work will give ground to entail numerical simulations that could use SAXS spectra as input parameters to get a deeper understanding of the mechanisms involved in the SLP decrease.

ACKNOWLEDGMENTS:

We acknowledge SOLEIL for provision of synchrotron radiation facilities and we would like to thank Dr. Javier Perez for assistance in using beamline SWING.

Supporting Informations Available

SI-1: Magnetization curve for bare nanoparticles. Langevin fit of the magnetization curve

SI-2: Dynamic light scattering correlation function for bare nanoparticles with corresponding fit at three pH values. Table containing the fit parameters.

SI-3: Form factor of bare nanoparticles obtain by SAXS, and the fit corresponding to normal distribution of polydisperse hard spheres.

SI-1 Magnetization curve for bare nanoparticles

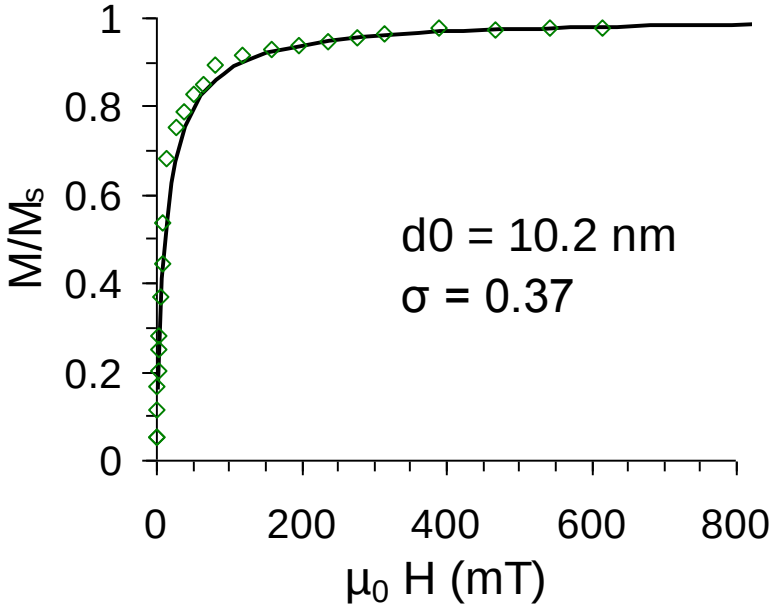

SI-2 Dynamic light scattering correlation function for bare nanoparticles with corresponding fit at three pH values.

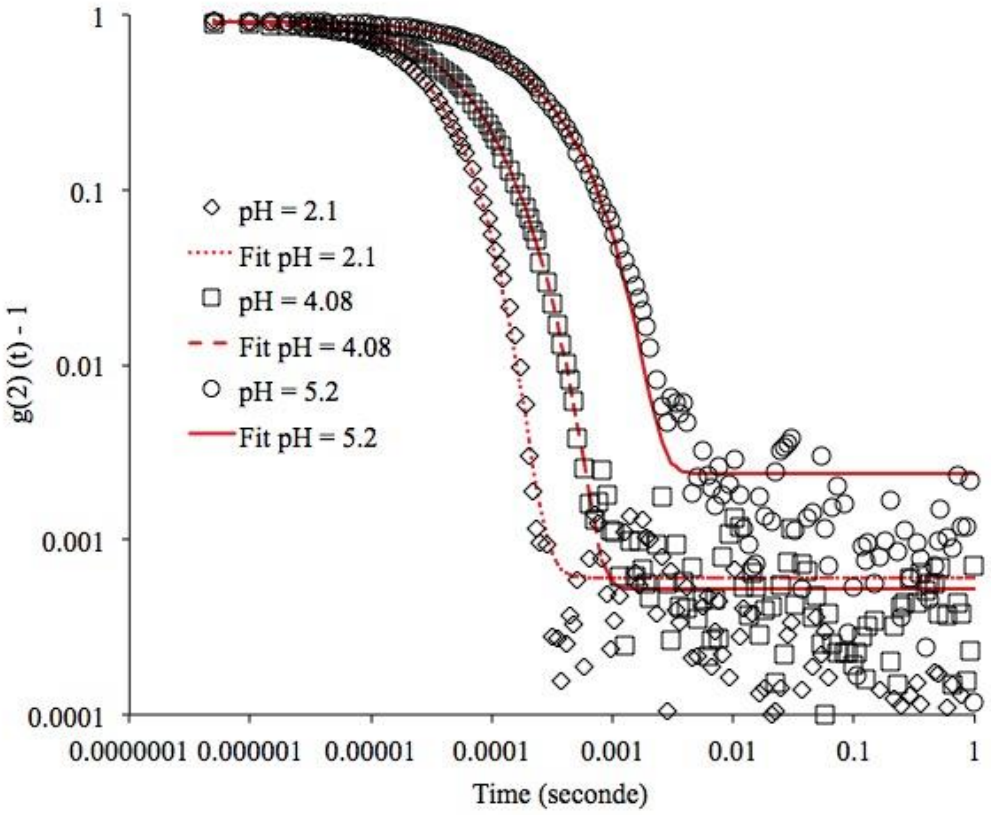

Table 1: Parameters of the fit:

pH	A_0	A_1	D_1 ($\mu m^2.s^{-1}$)	d_{H1} (nm)	$\%_{isolated}$	A_2	D_2 ($\mu m^2.s^{-1}$)	d_{H2} (nm)	$\%_{aggregated}$	d_{Hmean} (nm)
2.1	6.06E-04	0.91	4.41E-11	22.29	0.94	0.06	1.69E-11	58.04	0.06	24.33
4.08	5.24E-04	0.35	4.41E-11	22.29	0.37	0.60	1.71E-11	77.71	0.63	57.45
5.2	2.39E-03	0.21	1.27E-11	57.42	0.22	0.75	3.41E-12	288.60	0.78	238.15

SI-3 Form factor of bare nanoparticles obtain by SAXS

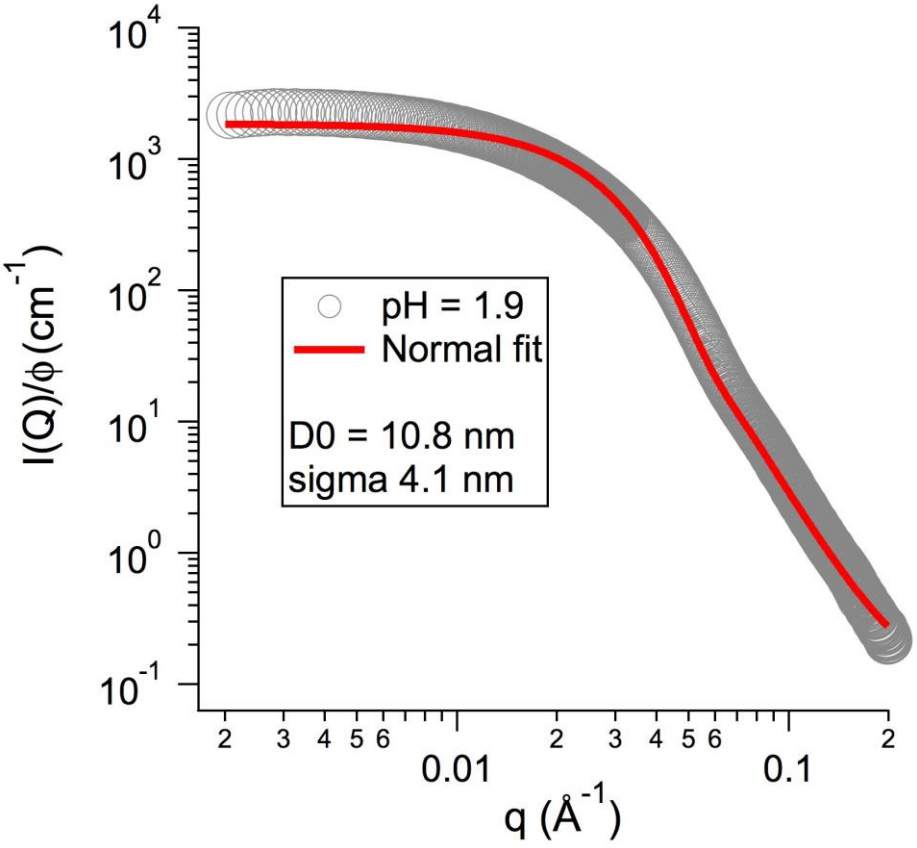
I(Q)/ϕ (cm-1)
q (Å-1)
pH = 1.9
Normal fit
D0 = 10.8 nm
sigma 4.1 nm

REFERENCES

(1) Jordan, A.; Scholz, R.; Wust, P.; Schirra, H.; Schiestel, T.; Schmidt, H.; Felix, R. Endocytosis of Dextran and Silan-Coated Magnetite Nanoparticles and the Effect of Intracellular Hyperthermia on Human Mammary Carcinoma Cells in Vitro. *J. Magn. Magn. Mater.* **1999**, *194* (1-3), 185–196.

(2) Johansson, F.; Jonsson, M.; Alm, K.; Kanje, M. *Exp Cell Res* **2010**, *316 (5)*, 688.

(4) Kumar, C.; Mohammad, F. Magnetic Nanomaterials for Hyperthermia-Based Therapy and Controlled Drug Delivery. *Adv. Drug Deliv. Rev.* **2011**, *63* (9), 789–808.

(5) Rosensweig, R. E. Heating Magnetic Fluid with Alternating Magnetic Field. *J. Magn. Magn. Mater.* **2002**, *252* (1-3), 370–374.

(6) Riedinger, A.; Guardia, P.; Curcio, A.; Garcia, M. A.; Cingolani, R.; Manna, L.; Pellegrino, T. Subnanometer Local Temperature Probing and Remotely Controlled Drug Release Based on Azo-Functionalized Iron Oxide Nanoparticles. *Nano Lett.* **2013**, *13* (6), 2399–2406.

(7) N'Guyen, T. T. T.; Duong, H. T. T.; Basuki, J.; Montembault, V.; Pascual, S.; Guibert, C.; Fresnais, J.; Boyer, C.; Whittaker, M. R.; Davis, T. P.; et al. Functional Iron Oxide Magnetic Nanoparticles with Hyperthermia-Induced Drug Release Ability by Using a Combination of Orthogonal Click Reactions. *Angew. Chem. Int. Ed.* **2013**, *52* (52), 14152–14156.

(8) Haase, C.; Nowak, U. Role of Dipole-Dipole Interactions for Hyperthermia Heating of Magnetic Nanoparticle Ensembles. *Phys. Rev. B* **2012**, *85* (4), 045435.

(9) Mehdaoui, B.; Tan, R. P.; Meffre, A.; Carrey, J.; Lachaize, S.; Chaudret, B.; Respaud, M. Increase of Magnetic Hyperthermia Efficiency due to Dipolar Interactions in Low-Anisotropy Magnetic Nanoparticles: Theoretical and Experimental Results. *Phys. Rev. B* **2013**, *87* (17), 174419.

(10) Deatsch, A. E.; Evans, B. A. Heating Efficiency in Magnetic Nanoparticle Hyperthermia. *J. Magn. Magn. Mater.* **2014**, *354* (0), 163–172.

(11) Béalle, G.; Di Corato, R.; Kolosnjaj-Tabi, J.; Dupuis, V.; Clément, O.; Gazeau, F.; Wilhelm, C.; Ménager, C. Ultra Magnetic Liposomes for MR Imaging, Targeting, and Hyperthermia. *Langmuir* **2012**, *28* (32), 11834–11842.

(12) Sadat, M. E.; Patel, R.; Sookoor, J.; Bud'ko, S. L.; Ewing, R. C.; Zhang, J.; Xu, H.; Wang, Y.; Pauletti, G. M.; Mast, D. B.; et al. Effect of Spatial Confinement on Magnetic Hyperthermia via Dipolar Interactions in Fe3O4 Nanoparticles for Biomedical Applications. *Mater. Sci. Eng. C* **2014**, *42*, 52–63.

(13) de Sousa, M. E.; Fernández van Raap, M. B.; Rivas, P. C.; Mendoza Zélis, P.; Girardin, P.; Pasquevich, G. A.; Alessandrini, J. L.; Muraca, D.; Sánchez, F. H. Stability and Relaxation Mechanisms of Citric Acid Coated Magnetite Nanoparticles for Magnetic Hyperthermia. *J. Phys. Chem. C* **2013**, *117* (10), 5436–5445.

(14) Chanteau, B.; Fresnais, J.; Berret, J. F. Electrosteric Enhanced Stability of Functional Sub-10 Nm Cerium and Iron Oxide Particles in Cell Culture Medium. *Langmuir* **2009**, *25* (16), 9064–9070.

(15) Massart, R. Preparation of Aqueous Magnetic Liquids in Alkaline and Acidic Media. *Magn.*

IEEE Trans. On **1981**, *17* (2), 1247–1248.

(16) Lefebure, S.; Dubois, E.; Cabuil, V.; Neveu, S.; Massart, R. Monodisperse Magnetic Nanoparticles: Preparation and Dispersion in Water and Oils. *J. Mater. Res.* **1998**, *13* (10), 2975–2981.

(17) Guibert, C.; Dupuis, V.; Fresnais, J.; Peyre, V. Controlling Nanoparticles Dispersion in Ionic Liquids by Tuning the pH. *J. Colloid Interface Sci.* **2015**, *454*, 105–111.

(18) Fresnais, J.; Yan, M.; Courtois, J.; Bostelmann, T.; Bée, A.; Berret, J.-F. Poly(acrylic Acid)-Coated Iron Oxide Nanoparticles: Quantitative Evaluation of the Coating Properties and Applications for the Removal of a Pollutant Dye. *J. Colloid Interface Sci.* **2013**, *395*, 24–30.

(19) Fresnais, J.; Berret, J. F.; Frka- Petesic, B.; Sandre, O.; Perzynski, R. Electrostatic Co- Assembly of Iron Oxide Nanoparticles and Polymers: Towards the Generation of Highly Persistent Superparamagnetic Nanorods. *Adv. Mater.* **2008**, *20* (20), 3877–3881.

(20) Branquinho, L. C.; Carrião, M. S.; Costa, A. S.; Zufelato, N.; Sousa, M. H.; Miotto, R.; Ivkov, R.; Bakuzis, A. F. Effect of Magnetic Dipolar Interactions on Nanoparticle Heating Efficiency: Implications for Cancer Hyperthermia. *Sci Rep* **2013**, *3,* 2887.

(21) Tan, R. P.; Carrey, J.; Respaud, M. Magnetic Hyperthermia Properties of Nanoparticles inside Lysosomes Using Kinetic Monte Carlo Simulations: Influence of Key Parameters and Dipolar Interactions, and Evidence for Strong Spatial Variation of Heating Power. *Phys. Rev. B* **2014**, *90* (21), 214421.

(22) Cousin, F.; Dubois, E.; Cabuil, V. Tuning the Interactions of a Magnetic Colloidal Suspension. *Phys Rev E J1 - PRE* **2003**, *68* (2), 021405.

TOC figure: